

A quantum algorithm for the solution of the 0-1 Knapsack problem

Sören Wilkening,^{1,2} Andreea-Iulia Lefterovici,¹ Lennart Binkowski,¹ Michael Perk,³ Sándor Fekete,³ and Tobias J. Osborne¹

¹*Institut für Theoretische Physik, Leibniz Universität Hannover, Germany*

²*Volkswagen AG, Berliner Ring 2, 38440 Wolfsburg*

³*Institut für Betriebssysteme und Rechnerverbund, Technische Universität Braunschweig, Germany*

Here we present two novel contributions for achieving quantum advantage in solving difficult optimisation problems, both in theory and foreseeable practice. (1) We introduce the “Quantum Tree Generator”, an approach to generate in superposition all feasible solutions of a given instance, yielding together with amplitude amplification the optimal solutions for 0-1-Knapsack problems. The QTG offers exponential memory savings and enables competitive runtimes compared to the state-of-the-art Knapsack solver COMBO for instances involving as few as 600 variables. (2) By introducing a high-level simulation strategy that exploits logging data from COMBO, we can predict the runtime of our method way beyond the range of existing quantum platforms and simulators, for various benchmark instances with up to 1600 variables. Combining both of these innovations, we demonstrate the QTG’s potential advantage for large-scale problems, indicating an effective approach for combinatorial optimisation problems.

I. INTRODUCTION

We have arrived at an inflection point in the development of quantum technology with global investment in quantum computation, driven by the promise of near-term quantum advantage, leading to an explosion of activity, both on the hardware and software levels. Quantum information processing devices, with a variety of architectures, from superconducting qubits^{1,2} and trapped ions³⁻⁶, through photonic platforms⁷⁻⁹, are being created at an unprecedented rate, with physical qubit numbers nearly doubling in the past year alone^{10,11}. It is entirely reasonable to expect in the next years that quantum information processing devices will comprise many thousands of physical qubits¹². This progress is, however, ameliorated by a series of engineering challenges, emerging from the effects of decoherence^{13,14}. The current error rates experienced by all extant quantum devices place them well above the fault tolerance threshold¹⁵ required for the effective deployment of quantum error correction¹⁶. Further critical roadblocks, depending on platform, also include the difficulties of implementing mid-circuit measurements¹⁷ and entangling gates¹⁸. While extremely demanding, there is no fundamental physics reason that these challenges will not be overcome, and so the first quantum computers capable of furnishing ideal logical qubits will appear in the next years.

That quantum computers deliver useful improved and accelerated solutions is expected in the long term when logical qubits are plentiful and cheap. Use cases here include quantum chemistry^{19,20} and materials simulation²¹, where quantum advantage is expected when we reach roughly 10K logical qubits²². However, in the near- and mid-term, the situation is subtle and nuanced. There is considerable optimism that combinatorial optimisation problems provide a rich class of use cases whose solutions quantum computers will improve²³. However, while it has been argued that quantum devices have already demonstrated accelerated solutions for

synthetic problems²⁴, there has been, to date, no conclusive demonstration of quantum advantage for realistic instances with respect to the *best classical approach*. Quantum heuristics currently do not provide competitive results when compared with the best-in-class classical solvers, such as CPLEX and Gurobi which routinely solve problems involving thousands of variables to *provable optimality*²⁵.

Combinatorial optimisation problems are typically NP-complete²⁶ so that the analysis of the performance of quantum heuristics such as the QAOA²⁷ is extremely difficult to carry out. Indeed, any general naive argument about the performance of a variational quantum method would likely fall afoul of well-understood barriers in complexity theory, such as the Razborov-Rudich theorem²⁸. Thus our only recourse to reasoning about quantum heuristics is via benchmarks, but here we are also snookered: We need large-scale functioning quantum devices in order to run realistic benchmarks, but these do not yet exist. Our only general recourse is to perform classical simulations of quantum methods. But these are limited to 20-30 qubits, which is far too few to evaluate the performance of a quantum heuristic against realistic benchmark instances (which typically would require somewhere between 100-10000 qubits).

In this paper, we directly take on the twin challenges of (1) developing a quantum method to solve combinatorial optimisation problems and (2) evaluating the performance of the method against benchmark instances. We target the Knapsack problem – the hydrogen atom of combinatorial optimisation problems – and develop a quantum method we christen Quantum Tree Generator (QTG) to generate all feasible solutions in superposition, which yields the optimal solution in concert with quantum amplitude amplification. In order to evaluate the performance of the QTG-based search on realistic benchmark instances, we also introduce what we call the *high-level simulator*: Extracting crucial logging

Box 1: Quantum Tree Generator

Input

Knapsack instance $KP_n(\mathbf{p}, \mathbf{z}; Z)$, feasible assignment \mathbf{y}

1. Initialize:

Initialize the three registers in the state $|0\rangle^A |Z\rangle^B |0\rangle^C$.

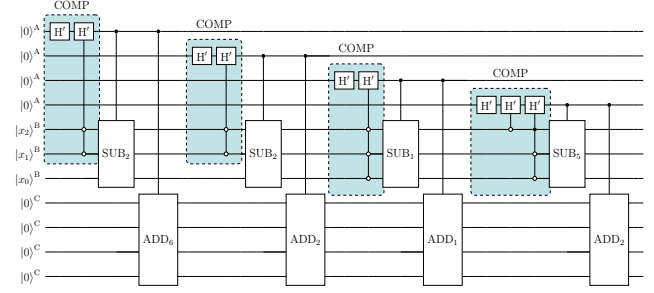
2. Tree traversing:

For each item $m = 1, \dots, n$, perform the following steps:

- (a) Create a superposition. Apply the biased Hadamard H' on the m -th qubit in register A, controlled on whether z_m does not exceed the remaining capacity stored in register B.
- (b) Update the remaining costs. Subtract z_m from the state of register B, controlled on the m -th qubit in register A.
- (c) Update the total profit. Add p_m to the state of register C, controlled on the m -th qubits in register A.

Example

Knapsack instance $KP_4(\mathbf{p}, \mathbf{z}; 7)$ with costs $\mathbf{z} = (2, 2, 1, 5)$ and profits $\mathbf{p} = (6, 2, 1, 2)$



data from the classical solution, obtained via the current champion COMBO method, we can infer the expected number of cycles required by the QTG-based method to solve the same instance (importantly, we cannot simulate the method, only infer the expected running time in elementary gates using this side information). This is the first time that the performance of a quantum algorithm on realistic benchmark instances has been evaluated. Our benchmarking leads us to predict that the QTG-based method requires fewer cycles to solve realistic instances already at 600 variables. Most dramatic, however, are the memory requirements: The COMBO method – based in part on dynamic programming – can make huge demands on memory, with 10^{10} bits being routinely requested. The QTG-based search, however, requires only a constant multiple of the variable number in logical qubits. This leads to a possible quantum advantage in both time and space for 600 variables.

II. PRELIMINARIES

Consider a set of n items, each of which has some integer profit $p_m > 0$ and cost $z_m > 0$. The objective is to select a subset of items of maximum cumulative profit, so that their cumulative costs do not exceed some threshold $Z > 0$. An instance of the 0-1-Knapsack Problem (or 0-1-KP for short) is completely defined by the number n of items, a list $\mathbf{p} := (p_1, \dots, p_n)$ of profit values, a list $\mathbf{z} := (z_1, \dots, z_n)$ of costs, and the capacity Z ; we address a given instance in the following by $KP_n(\mathbf{p}, \mathbf{z}; Z)$. It has the following formulation as an Integer Linear Program (ILP).

$$\begin{aligned}
 & \text{maximise} && \sum_{m=1}^n p_m y_m \\
 & \text{subject to} && \sum_{m=1}^n z_m y_m \leq Z \\
 & && y_m \in \{0, 1\}, \quad m = 1, \dots, n.
 \end{aligned} \tag{1}$$

For the 0-1-KP, the binary variable y_m encodes the choice of either including item m into the knapsack ($y_m = 1$) or omitting it ($y_m = 0$). Therefore, a complete assignment of all items (also called *path*) constitutes a bit string of length n .

The standard procedure to formulate the 0-1-KP for study via a quantum computer is to represent the paths $\mathbf{y} = y_1 \dots y_n$ as computational basis states $|\mathbf{y}\rangle^A$ in an n -qubit *path register* $\mathcal{H}_A = \mathbb{C}^{2^n}$. Therefore, each item corresponds to one qubit in this register. Additionally, for any feasible assignment \mathbf{y} , we store the binary representation of the remaining capacity $Z - \sum_{m=1}^n z_m y_m$ as a quantum state $|x_{\mathbf{y}}\rangle^B$ in a $\lceil \log_2 Z \rceil$ -qubit *capacity register* \mathcal{H}_B . The total profit is stored as a state $|P_{\mathbf{y}}\rangle^C$ in a $\lceil \log_2 P \rceil$ -qubit *profit register* \mathcal{H}_C , where P is any upper bound on the optimal profit. The total number of used qubits in the composite register $\mathcal{H} = \mathcal{H}_A \otimes \mathcal{H}_B \otimes \mathcal{H}_C$ is therefore given by

$$n + \lceil \log_2 Z \rceil + \lceil \log_2 P \rceil. \tag{2}$$

Our quantum algorithm for solving 0-1-KP operates entirely on the aforementioned composite register and a few ancilla qubits, thereby admitting a quasi-exponential memory saving relative to dynamic programming-based solvers like COMBO. The quantum routine is fundamentally based on two main ingredients:

1. a state preparation circuit that creates a superposition of all valid paths along with their total profit and remaining capacity as composite quantum states.
2. an augmented version of quantum amplitude amplification²⁹ which increases the success probability of measuring the optimal solution while avoiding endless loops.

III. METHODS

The entire state preparation circuit, the Quantum Tree Generator (QTG) \mathcal{G} , arises as a cascade of n layer uni-

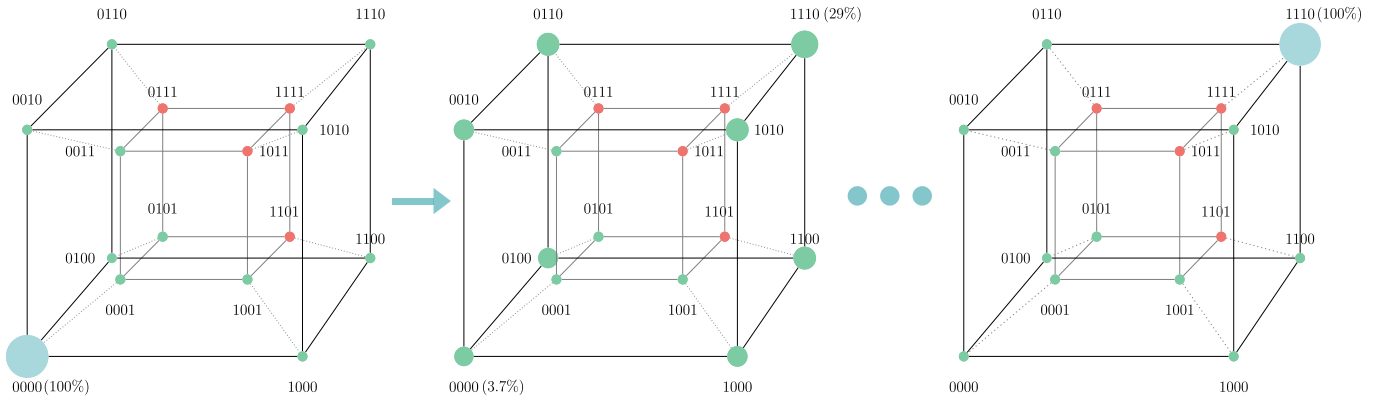


FIG. 1. The action of the QTG on the $KP_4(\mathbf{p}, \mathbf{z}; 7)$ example. The path register holds 16 computational basis states – here depicted as the corners of a hypercube – representing all feasible (green dots) and infeasible (orange dots) four-item paths. The state $|1110\rangle$ represents the optimal solution. The initial state of the system is $|0000\rangle$, corresponding to an entirely empty knapsack. After one application of the QTG, the optimal state’s sampling probability is increased to 29%. After 12 applications of the QTG, the optimal state is reached.

varies U_m , i.e., $\mathcal{G} = \prod_{m=1}^n U_m$. Applying the QTG to the initial state $|0\rangle^A |Z\rangle^B |0\rangle^C$ generates a (generally non-uniform) superposition of all valid paths. The QTG iteratively includes/excludes all items in a weighted superposition while checking for feasibility and updating the capacity and profit registers. First, for every path, it is checked whether the remaining capacity covers the cost of the current item m . Next, every path that can include the item will be branched using a biased Hadamard gate $H_b^{y_m}$ ³⁰ defined as

$$\begin{aligned} H_b^0 &= \frac{1}{\sqrt{b+2}} \begin{pmatrix} \sqrt{1+b} & 1 \\ 1 & -\sqrt{1+b} \end{pmatrix}, \\ H_b^1 &= \frac{1}{\sqrt{b+2}} \begin{pmatrix} 1 & \sqrt{1+b} \\ \sqrt{1+b} & -1 \end{pmatrix}, \end{aligned} \quad (3)$$

where y_m is the m -th bit of an intermediate solution \mathbf{y} . Upon successful item inclusion, the item’s cost is subtracted from the capacity register’s state and its profit is added to the profit register’s state. Both, subtraction and addition, are conducted using QFT adders³¹. In total, the unitaries U_m are comprised of three components $U_m = U_m^C U_m^B U_m^A$:

$$\begin{aligned} U_m^A &= C_{\geq z_m}^B (H_b^{y_m}) \\ U_m^B &= C_m^A (\text{SUB}_{z_m}) \\ U_m^C &= C_m^A (\text{ADD}_{p_m}), \end{aligned} \quad (4)$$

More details on the construction of the biased Hadamard gates $H_b^{y_m}$ and unitaries U_m can be found in Section VIA. The concept of the QTG is summarised in Box 1, along with the $KP_4(\mathbf{p}, \mathbf{z}; 7)$ circuit example.

The superposition created by the QTG is further manipulated in order to increase the probability of measuring the optimal solution states. For this, we employ quantum maximum finding (**QMaxSearch**)³², which iteratively calls an amplitude amplification (**QSearch**)²⁹

routine. The intermediate best solution’s total profit provides the current threshold and is therefore entirely evaluated on the third register. More details can be found in Section VIB.

The benchmark instances³³ are generated by Jookan et al.’s³⁵ instance generator. Due to the limitation of the quantum simulation, we obtain runtime results only for the “easy” instances, but we are able to compare at least the memory requirements of difficult instances. For the benchmark procedure, we select simulatable instances having between 200 and 1600 variables. We further choose a bias, based on the calculations in Section VIA, $b = n/4$ and a fixed maximum number of $M = 200$ Grover iterations within **QSearch**. In a classical preprocessing step, we sort the list of items by their efficiency, and obtain an initial threshold for **QMaxSearch** via Integer Greedy.

By combining the simulation of the application of the QTG (see Figure 1 for the $KP_4(\mathbf{p}, \mathbf{z}; 7)$ example), the phase flip operator within **QSearch**, and quantum measurements with a detailed analysis of the resource requirements of every subcircuit (Section VID), we calculate the number of necessary quantum cycles for obtaining the optimal solution with a certain success probability. Our analysis makes the following crucial assumptions:

1. all qubits and gates are noiseless, logical components.
2. all single-qubit gates, single-controlled single-qubit rotations, and Toffoli gates together constitute a universal set of gates of equal implementation cost.
3. disjoint gates can be executed in parallel, constituting a single cycle on the QPU.

More details can be found in Section VIC and Section VID. In contrast, the runtime and the memory usage of COMBO were gathered by straightforward execution on the selected instances and measuring the number

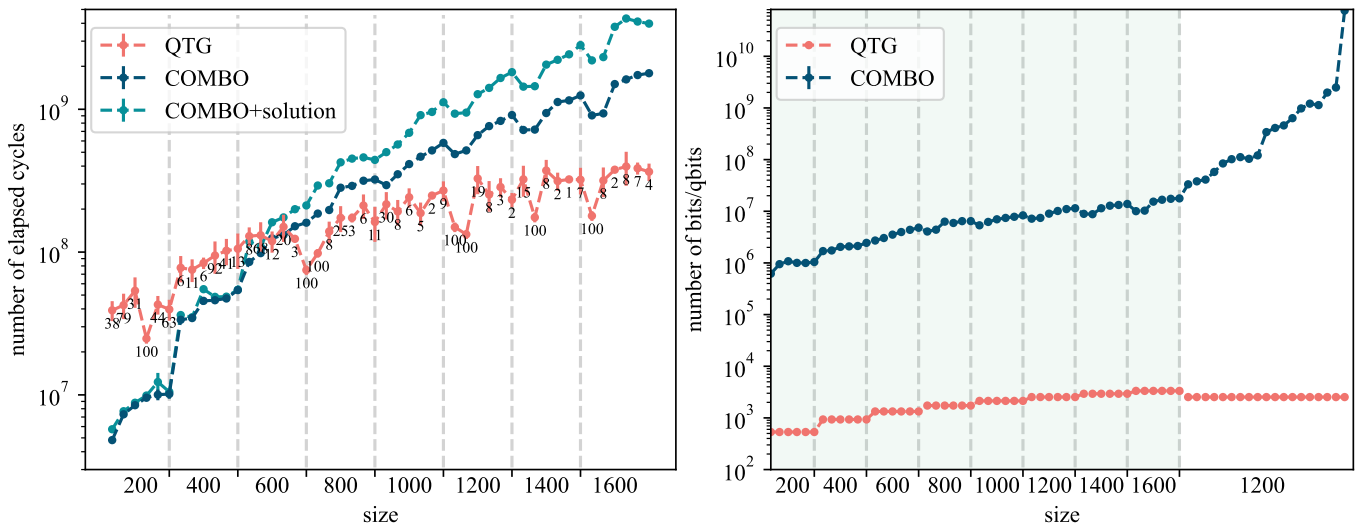


FIG. 2. QTG-based search vs. COMBO: performance and resource demands. We simulate the application of the QTG and **QMaxSearch** for benchmark instances^{33,34} having between $n = 200$ and $n = 1600$ variables with a bias $b = n/4$ and $M = 200$ Grover iterations. On the same large instances we execute COMBO, once only determining the optimal profit and once also producing an optimal assignment. **a)** The orange line shows the average number of elapsed quantum cycles for 100 runs of the QTG-based search, while the error bars depict the standard deviation. Because QTG-based search is a non-deterministic algorithm, the optimal solution is only sampled with a certain success probability recorded for every instance. Meanwhile, the blue lines show the average measured cycle count for executing COMBO 100 times with and without outputting an optimal assignment. The hardware fluctuations are negligible for higher runtimes and therefore result in vanishing error bars. Assuming comparability of classical and quantum cycles, we observe within the regime of 600 variable instances that QTG-based search starts outperforming COMBO at the expense of reduced but reasonable success probabilities. The trend continues towards larger instances and indicates a generally more favourable slope for the quantum method than for COMBO. Occasionally, all methods show dips in the required cycles, corresponding to instances where Integer Greedy gives the optimal solution. For those instances, the success probability of QTG-based search is already maximal. **b)** The orange line shows the number of qubits required for executing QTG-based search for the given instances. Its main contribution is due to (2), and all the ancilla qubits for gate decompositions etc. are accounted for. In comparison, the blue line shows the number of classical bits required for executing COMBO on the same instances. Assume for the moment comparability of bits and qubits, the initial requirement for COMBO is three orders of magnitude higher than for QTG-based search. For the simulatable instances (green background) the offset between both methods remains approximately the same. In the regime of non-simulatable instances with 1200 variables, the memory demands of COMBO quickly rise to 10GB while QTG-based search remains memory modest.

of elapsed processor cycles. As COMBO is a single-core algorithm, it makes the comparison of elapsed cycles a fair unit of measurement. The benchmarks were executed on a MacBook Pro 2019, with a 2.6 GHz 6-Core Intel Core i7 CPU and 16 GB 2667 MHz DDR4 memory.

IV. RESULTS

We demonstrate the capabilities of our QTG-based search on realistic benchmark instances up to 1600 variables (see Figure 2). We numerically observe that COMBO’s cycle demand overtakes the quantum method’s elapsed cycles already at instances with 600 variables and, overall, indicates a steeper slope.

Additionally, we observe that the QTG-based method requires far less memory than COMBO (assuming comparability of bits and qubits). While the number of involved qubits stays constant for instances of the same size, COMBO’s memory requirements explode with increasing problem hardness.

V. DISCUSSION AND CONCLUSIONS

In this paper we have proposed and investigated a quantum method for solving the 0-1-KP. Due to our high-level simulator, we were able to collect numerical data, rather than mere extrapolation, for benchmark instances with up to 1600 variables.

On the evaluated benchmarks, the quantum method admitted favourable runtimes for instances with at least 600 variables while also requiring a significantly smaller amount of memory. Both results together – runtime and (enormous) memory savings – hint at a possible practical quantum advantage for solving the 0-1-KP.

The only downside with which the runtime results must be viewed is the reduced success probabilities. However, by leveraging the reduced number of qubits in contrast to the classical memory, we can increase the success probability of the algorithm by executing **QMaxSearch** in parallel multiple times, without affecting the runtime of the QTG.

It is important to acknowledge that there exist several

other potential ways for improvement. These areas of potential enhancement encompass the utilisation of upper bound heuristics within the QTG to reduce branching, or the utilisation of a preprocessing branch-and-bound procedure, such that the QTG-based search is executed only on the remaining subsequent problem, or to use a different bias function based on the cost of the items.

ACKNOWLEDGMENTS

This work was supported by the DFG through SFB 1227 (DQ-mat), Quantum Frontiers, the Quantum Valley Lower Saxony, the BMBF projects ATIQ and QuBRA, and the BMWi project ProvideQ. Helpful correspondence and discussions with Arne-Christian Voigt, Mark Benne- mann, and Timo Ziegler are gratefully acknowledged.

AUTHOR CONTRIBUTIONS

This project was conceived of, and initiated in, discus- sions of S.W. and T.J.O. The quantum implementation along with the resource estimation procedures were de- veloped by S.W, L.B and A.I.L. The classical expertise was provided by S.F. and M.P. All authors contributed to writing the paper.

REFERENCES

- ¹M. Kjaergaard, M. E. Schwartz, J. Braumüller, P. Krantz, J. I.-J. Wang, S. Gustavsson, and W. D. Oliver, *Annual Review of Condensed Matter Physics* **11**, 369 (2020).
- ²I. Siddiqi, *Nature Reviews Materials* **6**, 875 (2021).
- ³R. Blatt and C. F. Roos, *Nature Physics* **8**, 277 (2012).
- ⁴J. I. Cirac and P. Zoller, *Physical review letters* **74**, 4091 (1995).
- ⁵H. Häffner, C. F. Roos, and R. Blatt, *Physics reports* **469**, 155 (2008).
- ⁶D. Leibfried, R. Blatt, C. Monroe, and D. Wineland, *Reviews of Modern Physics* **75**, 281 (2003).
- ⁷L. S. Madsen, F. Laudenbach, M. F. Askarani, F. Rortais, T. Vincent, J. F. Bulmer, F. M. Miatto, L. Neuhaus, L. G. Helt, M. J. Collins, *et al.*, *Nature* **606**, 75 (2022).
- ⁸S. Slussarenko and G. J. Pryde, *Applied Physics Re- views* **6** (2019).
- ⁹B.-H. Wu, R. N. Alexander, S. Liu, and Z. Zhang, *Phys- ical Review Research* **2**, 023138 (2020).
- ¹⁰I. News, *Ibm osprey - ibm's new 433-quantum bit (qubit) processor* (2022).
- ¹¹C. Q. Choi, *IEEE Spectrum* **60**, 46 (2023).
- ¹²G. Jay and S. Matthias, *Charting the course to 100,000 qubits* (2023).
- ¹³H. E. Brandt, *Progress in Quantum Electronics* **22**, 257 (1999).
- ¹⁴M. Schlosshauer, *Physics Reports* **831**, 1 (2019).
- ¹⁵J. Preskill, *Quantum* **2**, 79 (2018).
- ¹⁶D. A. Lidar and T. A. Brun, *Quantum error correction* (Cambridge university press, 2013).
- ¹⁷K. Rudinger, G. J. Ribeill, L. C. Govia, M. Ware, E. Nielsen, K. Young, T. A. Ohki, R. Blume-Kohout, and T. Proctor, *Phys. Rev. Appl.* **17**, 014014 (2022).
- ¹⁸M. Reagor, C. B. Osborn, N. Tezak, A. Staley, G. Prawiroatmodjo, M. Scheer, N. Alidoust, E. A. Sete, N. Didier, M. P. da Silva, *et al.*, *Science advances* **4**, eaao3603 (2018).
- ¹⁹Y. Cao, J. Romero, J. P. Olson, M. Degroote, P. D. Johnson, M. Kieferová, I. D. Kivlichan, T. Menke, B. Peropadre, N. P. Sawaya, *et al.*, *Chemical reviews* **119**, 10856 (2019).
- ²⁰B. P. Lanyon, J. D. Whitfield, G. G. Gillett, M. E. Goggin, M. P. Almeida, I. Kassal, J. D. Biamonte, M. Mohseni, B. J. Powell, M. Barbieri, *et al.*, *Nature chemistry* **2**, 106 (2010).
- ²¹B. Bauer, S. Bravyi, M. Motta, and G. K.-L. Chan, *Chemical Reviews* **120**, 12685 (2020).
- ²²T. Hoefler, T. Häner, and M. Troyer, *Commun. ACM* **66**, 82–87 (2023).
- ²³A. Ajagekar, T. Humble, and F. You, *Computers & Chemical Engineering* **132**, 106630 (2020).
- ²⁴F. Arute, K. Arya, R. Babbush, D. Bacon, J. C. Bardin, R. Barends, R. Biswas, S. Boixo, F. G. S. L. Brandao, D. A. Buell, *et al.*, *Nature* **574**, 505 (2019).
- ²⁵E.g., classical optimisation methods can, on a smart- phone, routinely solve the travelling salesman problem to provable optimality for hundreds of cities!
- ²⁶R. M. Karp, *Reducibility among Combinatorial Prob- lems* (Springer US, Boston, MA, 1972) pp. 85–103.
- ²⁷E. Farhi, J. Goldstone, and S. Gutmann, *A Quan- tum Approximate Optimization Algorithm* (2014), arXiv:1411.4028 [quant-ph].
- ²⁸A. A. Razborov and S. Rudich, *Journal of Computer and System Sciences* **55**, 24 (1997).
- ²⁹G. Brassard, P. Høyer, M. Mosca, and A. Tapp, *Con- temporary Mathematics* , 53 (2002).
- ³⁰For brevity, we also write H' when the parameters are either clear from the context or not relevant.
- ³¹T. G. Draper, *Addition on a Quantum Computer* (2000), arXiv:quant-ph/0008033 [quant-ph].
- ³²C. Durr and P. Høyer, *A Quantum Algorithm for Find- ing the Minimum* (1996), quant-ph/9607014.
- ³³J. Jooker, P. Leyman, and P. De Causmaecker, *Knap- sack problem instances* (2022).
- ³⁴*Qtg instances* (2023).
- ³⁵J. Jooker, P. Leyman, and P. De Causmaecker, *Euro- pean Journal of Operational Research* **301**, 841 (2022).
- ³⁶L. K. Grover, *A fast quantum mechanical algorithm for database search* (1996), quant-ph/9605043.
- ³⁷M. Boyer, G. Brassard, P. Høyer, and A. Tapp, *Fortschritte der Physik* **46**, 493 (1998).
- ³⁸M. Smelyanskiy, N. P. D. Sawaya, and A. Aspuru- Guzik, *qHiPSTER: The Quantum High Performance Software Testing Environment* (2016), 1601.07195

[quant-ph].

- ³⁹M. Matsumoto and T. Nishimura, *ACM Trans. Model. Comput. Simul.* **8**, 3–30 (1998).
- ⁴⁰D. Coppersmith, An approximate Fourier transform useful in quantum factoring (2002), [arXiv:quant-ph/0201067](https://arxiv.org/abs/quant-ph/0201067) [quant-ph].
- ⁴¹M. D. Ercegovic and T. Lang, *Digital Arithmetic* (Elsevier, 2004).

VI. SUPPLEMENTARY INFORMATION

A. Branching strategy

1. Biased Hadamard Gates

First we consider the biased Hadamard gates (3) and note that, for $b = 0$, both variants yield the usual (un-biased) Hadamard gate H . This would correspond to including or excluding the items with equal probability. Accordingly, we numerically observed that the number of elapsed quantum cycles for obtaining a reasonable success probability would generally not be competitive when using the usual Hadamard gates.

In comparison, allowing for biased Hadamard gates and fine-tuning the bias b can lead to an enormous speed-up during the phase of amplitude amplification: Given an intermediate solution \mathbf{y}' , whose profit also constitutes the current threshold for the **QMaxSearch**, we can actively favour feasible paths \mathbf{y} that have a certain Hamming distance $\Delta := \Delta(\mathbf{y}', \mathbf{y})$ to \mathbf{y} . Namely, applying the QTG and its biased Hadamard gates with arbitrary but fixed bias b , we can give the following lower bound on the sampling probability of \mathbf{y} :

$$|a_{\mathbf{y}}|^2 = \left(\frac{b+1}{b+2}\right)^{n-\Delta} \left(\frac{1}{b+2}\right)^{\Delta}. \quad (5)$$

This bound is tight if all possible branchings occur when constructing the path \mathbf{y} . For each bit in which \mathbf{y} and \mathbf{y}' differ, the application of a biased Hadamard gate introduces the prefactor $1/(b+2)$. For each of the remaining bits, it establishes the prefactor $(b+1)/(b+2)$.

Now, we can determine b in order to maximise the sampling probability of \mathbf{y} within the superposition created by the QTG. Differentiating (5) with respect to b and checking for zeros yield the optimal bias

$$b_{\text{opt}} = \frac{n}{\Delta} - 2 \approx \frac{n}{\Delta}. \quad (6)$$

Fine-tuning the bias in order to sample paths with a certain hamming distance more frequently helps searching the neighbourhood of good intermediate solutions for even better solutions. As a matter of fact, we observe that for many Knapsack instances the optimal solution and the Integer Greedy result do have a lot of common bit values, corresponding to items whose efficiency is just too good to not be included in any optimal assignment.

Because we employ Integer Greedy for obtaining an initial solution in our **QMaxSearch** routine, the biased Hadamard approach typically results in highly improved performance.

2. Construction of the layer unitaries

As described in Section III, the QTG is composed of the layer unitaries $U_m: \mathcal{G} = \prod_{m=1}^n U_m$. That is, each U_m manages the inclusion/exclusion of an item m . The unitaries U_m are themselves comprised of three components:

1. Create a biased superposition of including or excluding item m if and only if including the item does not exceed the capacity Z , otherwise do nothing. We achieve this step by applying a multi-controlled biased Hadamard gate to the m -th qubit. The Hadamard gate itself acts on the m -th qubit in the register \mathcal{H}_A . The control runs over the qubits of the second register \mathcal{H}_B and checks whether the remaining capacities cover the costs z_m of including item m . Accordingly, we denote the control with $C_{\geq z_m}^B$, because it asks whether the second register's state, interpreted as the binary representation of an integer, is greater or equal to the integer z_m . It then highly depends on the actual value of z_m which qubits in \mathcal{H}_B have to be involved into the control (see Section VID 5). In summary, this subgate is given by $U_m^A := C_{\geq z_m}^B (H_b^{y_m})$.
2. Update the remaining costs. For this, we have to perform an integer subtraction by z_m in the second register \mathcal{H}_B – denoted by SUB_{z_m} – which is, however, only executed if the main register \mathcal{H}_A represents a path for which the m -th item is included. That is, the integer subtraction by z_m is controlled by the m -th qubit in the main register. The entire update step therefore reads $U_m^B := C_m^A \text{SUB}_{z_m}$.
3. Update the total profit. Here, we perform an integer addition by p_m in the third register \mathcal{H}_C – denoted by ADD_{p_m} – which is, analogously to step 2, controlled by the m -th qubit in the main register. This last update step thus reads $U_m^C := C_m^A \text{ADD}_{p_m}$.

To give an explicit example: Let \mathbf{y} be a feasible path whose m -th bit is set to zero and let $\tilde{\mathbf{y}}$ be the same bit string, but with its m -th bit set to one. Further assume that the m -th bit of the intermediate solution \mathbf{y}' has the value one. The action of U_m on a the feasible product state $|\mathbf{y}\rangle^A |x_{\mathbf{y}}\rangle^B |P_{\mathbf{y}}\rangle^C$ then reads

$$U_m |\mathbf{y}\rangle^A |x_{\mathbf{y}}\rangle^B |P_{\mathbf{y}}\rangle^C = \begin{cases} |\mathbf{y}\rangle^A |x_{\mathbf{y}}\rangle^B |P_{\mathbf{y}}\rangle^C, & \text{if } x_{\mathbf{y}} < z_{n-m} \\ \sqrt{\frac{1}{b+2}} |\mathbf{y}\rangle^A |x_{\mathbf{y}}\rangle^B |P_{\mathbf{y}}\rangle^C + \sqrt{\frac{b+1}{b+2}} |\tilde{\mathbf{y}}\rangle^A |x_{\mathbf{y}} - z_m\rangle^B |P_{\mathbf{y}} + p_m\rangle^C, & \text{else.} \end{cases} \quad (7)$$

B. Quantum maximum finding

Here, we recap the known quantum algorithms Amplitude Amplification/**QSearch** and **QMaxSearch** and detail our adjustments for application to the 0-1-KP.

QSearch is a direct generalisation of Grover’s famous algorithm³⁶. More precisely, Grover’s algorithm was initially proposed for finding a unique marked state within a uniform superposition. It was then generalised to instances with multiple marked states in the form of the *quantum exponential searching algorithm*³⁷. The two central building blocks of these algorithms are the *phase oracle*

$$S_f |\mathbf{x}\rangle := (-1)^{f(\mathbf{x})} |\mathbf{x}\rangle, \quad (8)$$

which flips the phase of all states corresponding to bit strings \mathbf{x} that fulfill the Boolean trait $f(\mathbf{x}) = 1$, and the *diffusion operator*

$$D = H^{\otimes n} S_0 H^{\otimes n}. \quad (9)$$

In the more general **QSearch** routine, $H^{\otimes n}$ – which creates a uniform superposition of all computational basis states – is replaced by any other superposition creating unitary \mathcal{A} , in our case by the QTG \mathcal{G} . Fixing the Boolean function f and the state preparation unitary \mathcal{A} , the Amplitude Amplification operator is given by

$$Q := \mathcal{A} S_0 \mathcal{A}^\dagger S_f. \quad (10)$$

In the original proposal²⁹, the **QSearch** algorithm runs forever if there is no state \mathbf{x} fulfilling $f(\mathbf{x})$. In our case, however, this situation naturally occurs at the end of an entire **QMaxSearch** routine (see remainder of this section) which is why we additionally introduce a cut-off to prevent an endless loop. With this extension, our version of **QSearch** reads

Algorithm 1: **QSearch** (\mathcal{G} , f , M)

- 1 Set $l = 0$, $m_{\text{tot}} = 0$, and let c be any constant such that $1 < c < 2$;
 - 2 Increase l by 1 and set $m = \lceil c^l \rceil$;
 - 3 Apply \mathcal{G} to the initial state $|\mathbf{0}\rangle^A |Z\rangle^B |0\rangle^C$;
 - 4 Choose $j \in [1, m]$ uniformly at random and increase m_{tot} by $2j + 1$;
 - 5 Apply Q^j to the superposition
 $|s\rangle^{\text{ABC}} = \mathcal{G} |\mathbf{0}\rangle^A |Z\rangle^B |0\rangle^C$;
 - 6 Measure the register A and C, and get the outcome
 $|\mathbf{y}\rangle^A |P_{\mathbf{y}}\rangle^C$;
 - 7 **if** $f(P_{\mathbf{y}}) = 1$ or $m_{\text{tot}} \geq M$ **then**
 - 8 | return \mathbf{y} , $P_{\mathbf{y}}$;
 - 9 **else**
 - 10 | go to step 2;
 - 11 **end**
-

Because we are interested in maximising the total profit among all feasible paths, we have to choose the

Boolean function f accordingly. The apt method in question is provided by Quantum Maximum Finding. While initially proposed as an extension to Grover’s algorithm, its principle is directly transferable to **QSearch**.

The key idea is to introduce the comparison “ $P_{\mathbf{y}} > T$ ” as Boolean function which marks all paths \mathbf{y} whose total profit $P_{\mathbf{y}}$ exceeds a given threshold T . Starting with an initial threshold T_0 , **QSearch**(\mathcal{G} , $P_{\mathbf{y}} > T_0$, M) yields an intermediate solution $(\mathbf{y}_1, P_{\mathbf{y}_1})$. If $P_{\mathbf{y}_1} > T_0$, we can call **QSearch** again with the updated threshold $T_1 := P_{\mathbf{y}_1}$ and so on. However, if we obtain an output $(\mathbf{y}_i, P_{\mathbf{y}_i})$ with $P_{\mathbf{y}_i} \leq T_{i-1}$ throughout this routine, we can conclude – within a certain probability – that no valid path exists with a higher total profit than T_{i-1} ; hence we declare the previous intermediate solution $(\mathbf{y}_{i-1}, T_{i-1})$ the optimal solution. Because this case eventually occurs for every instance, we have introduced the additional termination condition in **QSearch**. Finally, for the initial threshold we employ the very efficient Integer Greedy method.

Algorithm 2: **QMaxSearch**(\mathcal{G} , M , \mathbf{p} , \mathbf{z})

- 1 Calculate initial threshold T using Greedy: \mathbf{y}_{out} ,
 $T = \text{intGr}(\mathbf{p}, \mathbf{z}, Z)$;
 - 2 **while** True **do**
 - 3 | \mathbf{y} , $P_{\mathbf{y}} = \text{QSearch}(\mathcal{G}, P_{\mathbf{y}} > T, M)$;
 - 4 | **if** $P_{\mathbf{y}} > T$ **then**
 - 5 | | set $T = P_{\mathbf{y}}$ and $\mathbf{y}_{\text{out}} = \mathbf{y}$;
 - 6 | **else**
 - 7 | | return \mathbf{y}_{out} , T ;
 - 8 | **end**
 - 9 **end**
-

C. High-level simulator

The instance sizes considered in Figure 2 are way too large for any conventional simulator which is based on evaluating the action of general quantum gates on general quantum states. Even with the most sophisticated simulation technique and with the aid of the largest available super computer, these approaches could only tackle up to 49 qubits³⁸. Instead, we developed a completely different high-level simulator tailored explicitly to the application of the QTG and **QMaxSearch**. The simulator consists of two main parts:

1. simulating the QTG while only storing computational basis states whose objective value surpasses the current threshold imposed by **QMaxSearch**.
2. simulating the application of the Amplitude Amplification operator via analytical formulas.

1. Simulated QTG

We simulate the QTG by exploring the classical binary decision tree for a given Knapsack instance using

breadth-first search (BFS) and, in doing so, keep track of the remaining costs, the total profit, and the sampling probabilities of the computational basis states after each application of one layer operator U_m . The sampling probabilities are propagated as follows: Assume a node in the m -th layer carries a remaining cost of x , a total profit of p , and a sampling probability of q . If $z_{m+1} > x$, no branching occurs and the only child node inherits its data from its parent node. If instead $z_{m+1} \leq x$, a branching produces two child nodes corresponding to either excluding (left) or including (right) the $(m+1)$ -th item. The child nodes' metadata are:

$$\begin{aligned} (x_{\text{left}}, x_{\text{right}}) &= (x, x - z_{m+1}) \\ (p_{\text{left}}, p_{\text{right}}) &= (p, p + p_{m+1}) \\ (q_{\text{left}}, q_{\text{right}}) &= \begin{cases} \left(\frac{q(b+1)}{b+2}, \frac{q}{b+2}\right), & \text{if } y_{m+1} = 0 \\ \left(\frac{q}{b+2}, \frac{q(b+1)}{b+2}\right), & \text{else.} \end{cases} \end{aligned}$$

The update rule for the child nodes' sampling probability directly results from the definition of the biased Hadamard gate (3).

During the BFS, we prune infeasible subtrees as the QTG would do anyway on a real quantum device, thereby massively reducing the final number of states. Furthermore, we also discard subtrees which do not admit any path with an objective value surpassing the current threshold. For this, we execute COMBO on the Knapsack subinstance that remains when fixing the first m decision variables y_1, \dots, y_m with the values corresponding to the current node in the decision tree. This yields a tight upper bound for the optimal profit achievable within the respective subtree. This second pruning step, although computationally sumptuous, reduces the final number of states in such a drastic way that even for large instances up to 1600 variables, only a few million – instead of 2^{1600} – states remain.

The result of this high-level QTG simulator, given a threshold T , is an array of paths (bit strings) together with their remaining capacity, total profit, and the theoretical sampling probability of the associated computational basis state. All these paths are feasible and admit, by construction, a respective total profit above the threshold T . This final array of states now serves as the input for the simulated Amplitude Amplification.

We denote this set of paths by \mathcal{F}^T and have therefore gained a representation of the superposition

$$\begin{aligned} |s\rangle^{\text{ABC}} &= \mathcal{G} |\mathbf{0}\rangle^{\text{A}} |Z\rangle^{\text{B}} |0\rangle^{\text{C}} \\ &= \sum_{\mathbf{y} \in \mathcal{F}^T} a_{\mathbf{y}} |\mathbf{y}\rangle^{\text{A}} |x_{\mathbf{y}}\rangle^{\text{B}} |P_{\mathbf{y}}\rangle^{\text{C}} + a_R |R\rangle \\ &= a_T |\mathcal{F}^T\rangle + a_R |R\rangle, \end{aligned}$$

where

$$|a_T|^2 := \sum_{\mathbf{y} \in \mathcal{F}^T} |a_{\mathbf{y}}|^2 \text{ and } |a_R|^2 = 1 - |a_T|^2.$$

All other feasible paths, but with a total profit below or equal to T , are thus collectively represented by the remainder state $|R\rangle$. In most cases, the remainder state's amplitude is nonzero, such that the cumulative sampling probability $q_T := |a_T|^2$ of all the paths in \mathcal{F}^T is not given by one.

2. Simulated Amplitude Amplification

Beside the QTG, we also have to simulate the action of the Amplitude Amplification operator \mathcal{Q} (step 5 in **QSearch**) and quantum measurements (step 6 in **QSearch**). Choosing some power $j \in \mathbb{N}$, the action of \mathcal{Q}^j on $|s\rangle^{\text{ABC}}$ is explicitly given²⁹ by

$$\begin{aligned} \mathcal{Q}^j |s\rangle^{\text{ABC}} &= \frac{\sin((2j+1) \arcsin(\sqrt{q_T}))}{\sqrt{q_T}} |\mathcal{F}^T\rangle \\ &+ \frac{\cos((2j+1) \arcsin(\sqrt{q_T}))}{\sqrt{1-q_T}} |R\rangle. \end{aligned} \quad (11)$$

The crucial aspect lies in the amplification of the amplitudes of the all the states contributing to the superposition $|\mathcal{F}^T\rangle$ – although being nonuniformly distributed – by the same factor. Therefore, the entire simulation of the action of \mathcal{Q}^j consists of merely multiplying each probability handed over by the high-level QTG simulator with the common amplification factor

$$\frac{\sin^2((2j+1) \arcsin(\sqrt{q_T}))}{q_T}. \quad (12)$$

Finally, simulating a quantum measurement in this framework is straightforward: Uniformly draw a random number from the interval $[0, 1]$ (we use GNU Scientific Library's implementation of the MT19937 algorithm³⁹). Then iteratively sum up the sampling probabilities of all the paths in \mathcal{F}^T until the cumulative probability surpasses the random number. If this occurs before the loop ends, the last added path is considered to have been measured and is returned (lines 7 and 8 in **QSearch**). Otherwise, that is if the random number exceeds q_T , we consider the remainder state being sampled (lines 9 and 10 in **QSearch**). Because in the latter case, we simply omit the result and restart the entire procedure with a new value for j , no further information is necessary. This completely justifies our approach of neglecting all the information about feasible states that admit a total profit below the given threshold.

D. Resource estimation

This section contains detailed resource estimations for the subcircuits required for implementing the QTG-based search, specifically, the costs associated with implementing the exploration unitaries $U_m = U_m^{\text{C}} U_m^{\text{B}} U_m^{\text{A}}$,

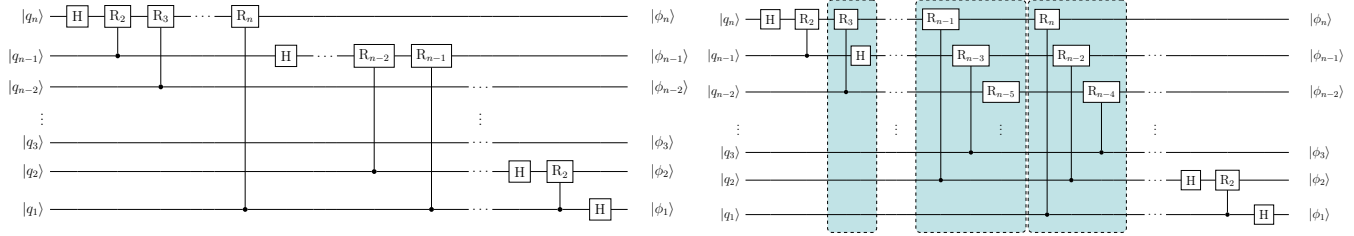


FIG. 3. **a)** The standard, nonparallelised QFT circuit. **b)** The optimally parallelised QFT circuit. For all $i = 3, \dots, n$, the gates in the $|q_{i-1}\rangle$ -level are shifted to the left until the leftmost gate, the Hadamard gate, is executed in parallel with the R_3 gate in the $|q_i\rangle$ -level. As the $|q_2\rangle$ -level does not admit an R_3 gate, the Hadamard gate in the $|q_1\rangle$ -level is executed alone. Therefore, for all $i = 2, \dots, n$, the $|q_{i-1}\rangle$ -level gate sequence with its $i - 1$ gates starts two layers after the $|q_i\rangle$ -level's sequence which is comprised of i gates. Starting from the $|q_n\rangle$ -level, each additional level thus introduces only one additional layer to the circuit.

$m = 1, \dots, n$. A crucial aspect of evaluating the efficiency of our quantum algorithm is to determine the total number of qubits \mathbf{Q} , gates \mathbf{G} , and cycles \mathbf{C} required for its implementation. Here, a cycle refers to a collection of gates that can be executed in parallel. In the context of resource estimation, we make the following assumptions:

- (i) Any n -controlled single-qubit gate can be decomposed into $2(n - 1)$ Toffoli gates and a single-controlled single-qubit gate. This decomposition utilises $n - 1$ ancilla qubits.
- (ii) All multi-controlled single-qubit gates that act on the same register have access to the same ancilla qubits arising from (i). This corresponds to taking the maximum instead of the sum of all additionally introduced ancilla qubits.
- (iii) It is equally expensive to have a controlled gate on the logical state 0 or 1.

1. Qubit count

The total number of qubits is given by the sum of the main registers' sizes (2) and the number of ancilla qubits for decomposing multi-controlled gates according to (i). Specifically, the size of the path register corresponds to the number of items involved in the Knapsack problem

$$\mathbf{Q}_{\text{PATH}} = n. \quad (13)$$

The size of the capacity register is determined by length of the capacity's binary representation, i.e.,

$$\mathbf{Q}_{\text{CAPACITY}} = \lceil \log_2 Z \rceil. \quad (14)$$

Analogously, given an upper bound P for the optimal profit, the size of the profit register is given by the length of P 's binary representation, that is

$$\mathbf{Q}_{\text{PROFIT}} = \lceil \log_2 P \rceil. \quad (15)$$

Additionally, the QTG contains the comparisons “ $x \geq z_m$ ” for all the item costs z_m , $m = 1, \dots, n$, which

constitute multi-controlled single-qubit gates (see Section VID5). Applying (i), the decomposition of those gates introduces up to $\lceil \log_2 Z \rceil - 1$ ancilla qubits. For simplicity, we assume that this upper bound is actually achieved by at least one of the comparisons. Due to assumption (ii), this number of ancilla qubits then suffices to implement all the comparisons. Analogously, the Amplitude Amplification operator \mathcal{Q} contains the phase oracles \mathcal{S}_0 and $\mathcal{S}_{P_{y>T}}$ which we realise using $\lceil \log_2 P \rceil$ -controlled single-qubit gates (see Section VID5). Hence, following (i) and (ii), $\lceil \log_2 P \rceil - 1$ additional ancilla qubits have to be introduced. Utilising (ii) again, these ancilla qubits then even suffice to execute \mathcal{Q} several times and with different thresholds T . Lastly, we use one additional qubit to store the potential phase flip applied by \mathcal{Q} . In total, we obtain an amount of

$$\begin{aligned} \mathbf{Q}_{\text{ANC}} &= (\lceil \log_2 Z \rceil - 1) + (\lceil \log_2 P \rceil - 1) + 1 \\ &= \lceil \log_2 Z \rceil + \lceil \log_2 P \rceil - 1 \end{aligned} \quad (16)$$

ancilla qubits. In summary, our methods requires the following number of qubits:

$$\begin{aligned} \mathbf{Q}_{\text{TOTAL}} &= \mathbf{Q}_{\text{PATH}} + \mathbf{Q}_{\text{CAPACITY}} + \mathbf{Q}_{\text{PROFIT}} + \mathbf{Q}_{\text{ANC}} \\ &= n + 2\lceil \log_2 Z \rceil + 2\lceil \log_2 P \rceil - 1. \end{aligned} \quad (17)$$

2. QFT

The well-known Quantum Fourier Transform⁴⁰ (QFT) plays a pivotal role for an efficient implementation of quantum adders (see Section VID3 and Section VID4) which we employ within the QTG. Figure 3 shows the general circuit representation of the QFT – unparallelised and parallelised – with shorthand notation

$$R_k := \begin{bmatrix} 1 & 0 \\ 0 & e^{2\pi i/2^k} \end{bmatrix}.$$

Gate count. The number of gates involved in the QFT is fully determined by the underlying register's size. Namely, to perform the QFT on the capacity register, the

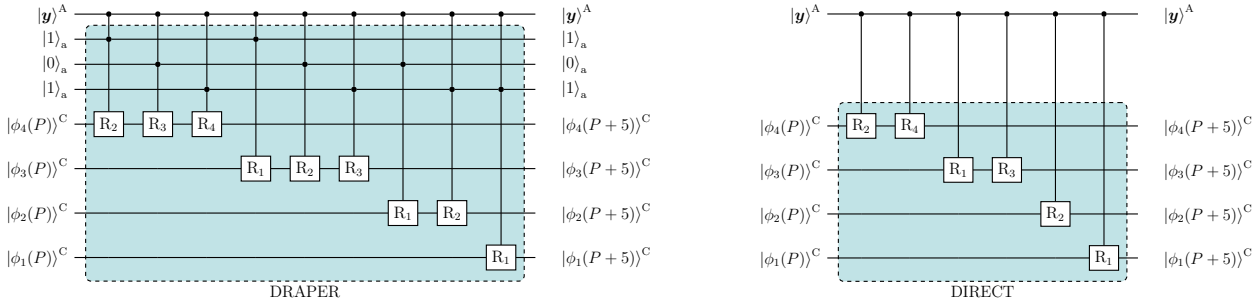


FIG. 4. Addition of the item profit $p_m = 5$ to the QFT-ed profit register, controlled on the m -th qubit in the path register. **a)** Draper method. The binary representation of the integer 5 is encoded into the three-qubit ancilla state $|101\rangle_a$ whose qubits control the application of the rotations R_k on the profit register. **b)** Direct method. The rotations for which the controlling ancilla qubit in Draper’s method would be in the $|1\rangle_a$ state are directly implemented, the remaining ones simply omitted. In comparison to Draper’s method, this saves several gates and the overall ancilla state preparation.

total number of gates required is given by

$$\mathbf{G}_{\text{QFT-CAPACITY}} = \frac{\lceil \log_2 Z \rceil (\lceil \log_2 Z \rceil + 1)}{2}. \quad (18)$$

Similarly, for the profit register, the total number of gates needed for the QFT is

$$\mathbf{G}_{\text{QFT-PROFIT}} = \frac{\lceil \log_2 P \rceil (\lceil \log_2 P \rceil + 1)}{2}. \quad (19)$$

Cycle count. Following the parallelisation strategy depicted in Figure 3, the number of cycles can be significantly reduced: The level-specific gate sequences can be shifted such that each level merely introduces one additional cycle to the nonparallelisable gate sequence in the highest level. As the length of the latter is given by the underlying register’s size, we derive the following formulas for the optimised QFT cycle count:

$$\mathbf{C}_{\text{QFT-CAPACITY}} = 2\lceil \log_2 Z \rceil - 1, \quad (20)$$

$$\mathbf{C}_{\text{QFT-PROFIT}} = 2\lceil \log_2 P \rceil - 1. \quad (21)$$

3. QFT Adder

Our version of the QFT adder is derived from the original proposal by Draper³¹. The latter is designed to add together two integers n_1 and n_2 which are encoded into quantum states $|n_1\rangle$ and $|n_2\rangle$ on two different registers. The result $|n_1 + n_2\rangle$ is then stored in, say, the first register. The entire QFT adder circuit consists of applying the QFT to the first register, then performing a cascade of rotations on the first register, controlled on the qubits of the second register, and finally applying the inverse QFT to the first register (see Figure 4 for an example on the profit register with additional control on some qubit in the path register). Because the items’ profits that we wish to add are known in advance, we can instead remove the controls and implement all the rotations, controlled on qubits which would have been initialised in the $|1\rangle$, directly. Figure 4 also shows an example of this variant of the addition step which, in comparison to Draper’s method, requires fewer gates and no ancilla qubits.

Gate count. The number of actually implemented gates in the addition step depends on the main register’s size and the number we wish to add, more precisely, on the position of ones in its binary representation: In the original proposal of Draper, the i -th qubit in the summand’s register controls $S - i + 1$ rotations in the main register, where S is the size of the main register. In the direct method, those $S - i + 1$ gates are implemented if and only if the i -th qubit is in the $|1\rangle$ state, that is if and only if the classical i -th bit is one. For a given profit p_m , let $(p_m)_i$ denote its i -th bit; the gate count for adding p_m to the QFT-ed profit register is then given by

$$\mathbf{G}_{\text{DIRECT}_{p_m}} = \sum_{i=0}^{\lceil \log_2 p_m \rceil} (\lceil \log_2 P \rceil + 1 - i)(p_m)_i. \quad (22)$$

Including the QFT and its inverse in the overall gate count for the additions, we obtain the following gate count for the QFT adder which adds the number p_m to the profit register:

$$\begin{aligned} \mathbf{G}_{\text{ADD}_{p_m}} &= 2\mathbf{G}_{\text{QFT-PROFIT}} + \mathbf{G}_{\text{DIRECT}_{p_m}} \\ &= \lceil \log_2 P \rceil (\lceil \log_2 P \rceil + 1) \\ &\quad + \sum_{i=1}^{\lceil \log_2 p_m \rceil} (\lceil \log_2 P \rceil + 1 - i)(p_m)_i. \end{aligned} \quad (23)$$

In the QTG circuit, all the additions on the profit registers are consecutive (see Figure 5) which allows for cancelling the inverse QFT within ADD_{p_m} and the QFT in $\text{ADD}_{p_{m+1}}$ for all $m = 1, \dots, n - 1$. As a result, only one QFT and one inverse QFT are applied to the profit register in total. The overall gate count for the addition of all item profits therefore reads

$$\begin{aligned} \mathbf{G}_{\text{ADD}_p} &= 2\mathbf{G}_{\text{QFT-PROFIT}} + \sum_{m=1}^n \mathbf{G}_{\text{DIRECT}_{p_m}} \\ &= \lceil \log_2 P \rceil (\lceil \log_2 P \rceil + 1) \\ &\quad + \sum_{m=1}^n \sum_{i=1}^{\lceil \log_2 p_m \rceil} (\lceil \log_2 P \rceil + 1 - i)(p_m)_i. \end{aligned} \quad (24)$$

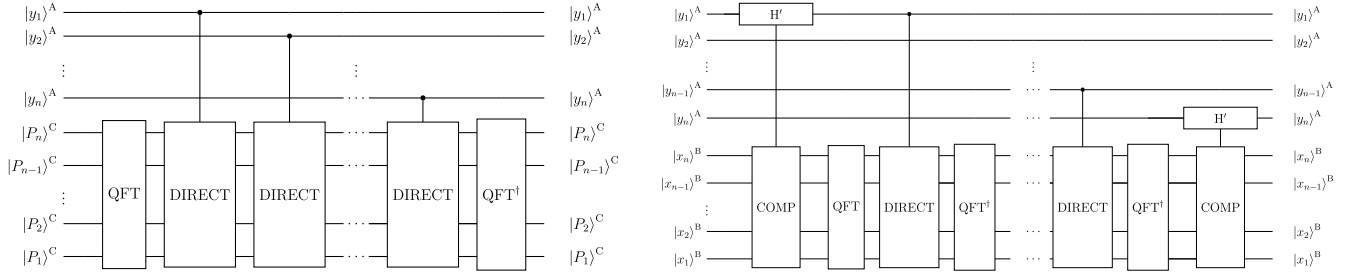


FIG. 5. **a)** The subcircuit performing all the profit additions. The profit register is QFT-ed in the beginning. Subsequently, the respective item profits are added via the direct method. The controlled Hadamard gates and the cost subtraction between the single additions are not depicted. After all item profits are added, the register is transformed back. **b)** The subtraction circuit including the comparison part. The biased Hadamard gates on the path register are controlled on the capacity register by integer comparisons. After the comparison the item costs are subtracted from the capacity register, controlled on the qubit just affected by the biased Hadamard gate. Because of this alternating involvement of the capacity register, the intermediate QFTs and their inverses do not cancel each other.

Cycle count. Within the QTG, any ADD_{p_m} is entirely controlled by the m -th qubit in the path register, respectively. This makes any further parallelisation within the actual addition part impossible. However, we can at least drop the control on the QFT and inverse QFT. In summary, we obtain here

$$\begin{aligned} \mathbf{C}_{\text{ADD}_p} &= 2\mathbf{C}_{\text{QFT-PROFIT}} + \sum_{m=1}^n \mathbf{G}_{\text{DIRECT}_{p_m}} \\ &= 4\lceil \log_2 P \rceil - 2 \\ &\quad + \sum_{m=1}^n \sum_{i=1}^{\lceil \log_2 p_m \rceil} (\lceil \log_2 P \rceil + 1 - i)(p_m)_i. \end{aligned} \quad (25)$$

4. QFT Subtractor

By flipping all the rotations' signs, the QFT adder circuit can also be employed for subtracting a given integer. Therefore, adding and subtracting both yield the same gate count.

Gate count. For a given profit z_m , let $(z_m)_i$ denote its i -th bit; the gate count for subtracting z_m from the QFT-ed capacity register is then given by

$$\mathbf{G}_{\text{DIRECT}_{z_m}} = \sum_{i=1}^{\lceil \log_2 z_m \rceil} (\lceil \log_2 Z \rceil + 1 - i)(z_m)_i. \quad (26)$$

Analogous to the QFT adder, including the QFT and its inverse in the overall gate count for the subtractions, we obtain the following gate count for the QFT subtractor which subtracts the number z_m from the capacity register

$$\begin{aligned} \mathbf{G}_{\text{SUB}_{z_m}} &= 2\mathbf{G}_{\text{QFT-CAPACITY}} + \mathbf{G}_{\text{DIRECT}_{z_m}} \\ &= \lceil \log_2 Z \rceil (\lceil \log_2 Z \rceil + 1) \\ &\quad + \sum_{i=1}^{\lceil \log_2 z_m \rceil} (\lceil \log_2 Z \rceil + 1 - i)(z_m)_i. \end{aligned} \quad (27)$$

Unlike the profit additions, the cost subtractions in the QTG circuit are followed by a comparison procedure, respectively, hence the intermediate QFT and inverse QFT do not cancel each other (see Figure 5). To reduce the number of gates, however, we omit the last subtraction SUB_{z_n} , because the capacity register is not checked again after the last item inclusion. All together, this leads to a total gate count of

$$\begin{aligned} \mathbf{G}_{\text{SUB}_z} &= 2n\mathbf{G}_{\text{QFT-CAPACITY}} + \sum_{m=1}^{n-1} \mathbf{G}_{\text{DIRECT}_{z_m}} \\ &= n\lceil \log_2 Z \rceil (\lceil \log_2 Z \rceil + 1) \\ &\quad + \sum_{m=1}^{n-1} \sum_{i=1}^{\lceil \log_2 z_m \rceil} (\lceil \log_2 Z \rceil + 1 - i)(z_m)_i. \end{aligned} \quad (28)$$

Cycle count. Because any SUB_{z_m} is also controlled by the m -th qubit in path register we obtain, in analogy to the QFT adder, a total cycle count of

$$\begin{aligned} \mathbf{C}_{\text{SUB}_z} &= 2n\mathbf{C}_{\text{QFT-CAPACITY}} + \sum_{m=1}^{n-1} \mathbf{G}_{\text{DIRECT}_{z_m}} \\ &= 4n\lceil \log_2 Z \rceil - 2n \\ &\quad + \sum_{m=1}^{n-1} \sum_{i=1}^{\lceil \log_2 z_m \rceil} (\lceil \log_2 Z \rceil + 1 - i)(z_m)_i. \end{aligned} \quad (29)$$

5. Comparison

Within the QTG-based search, there are three subcircuits requiring the comparison of two integers: First, the biased Hadamard gates within the QTG should only be executed if the remaining capacity in the second register is at least as large as the respective item cost. Therefore, we have to implement the integer comparisons “ $x \geq z_m$ ” with unknown x , but known z_m , $m = 1, \dots, n$. Second, the Amplitude Amplification operator \mathcal{Q} contains the reflection \mathcal{S}_0 , which flips the ancilla qubit's state if and

only if the profit register is in the $|0\rangle^C$ state. Third, the threshold-dependent phase oracle within the Amplitude Amplification operator flips the ancilla state, if and only if the third register enables a profit larger than the current threshold. That is, for known thresholds T and unknown p , we have to implement the comparisons “ $p > T$ ”.

We realise all the above operations as multi-controlled single-target gates. The control circuit is derived from the classical digital comparator⁴¹: Given two binary represented integers $a = a_\ell \dots a_1$ and $b = b_\ell \dots b_1$, introduce the Boolean variables

$$c_i := a_i b_i \vee \bar{a}_i \bar{b}_i, \quad (30)$$

which are 1 if and only if $a_i = b_i$, respectively. Then equality and strict inequalities in both directions can be expressed as

$$(a = b) = \bigwedge_{i=1}^{\ell} c_i, \quad (31)$$

$$(a > b) = \bigvee_{i=1}^{\ell} \left(a_i \bar{b}_i \bigwedge_{j=i+1}^{\ell} c_j \right), \quad (32)$$

$$(a < b) = \bigvee_{i=1}^{\ell} \left(\bar{a}_i b_i \bigwedge_{j=i+1}^{\ell} c_j \right). \quad (33)$$

If the integer b is known, the variables (30) can be reduced to a single literal, leaving (31)–(33) in orthogonal disjunctive normal form (ODNF). In addition, for $(a > b)$ only those clauses contribute for which \bar{b}_i is 1, i.e., b_i is 0. Analogously, for $(a < b)$ only those clauses contribute for which b_i is 1.

There are now two possibilities when implementing an operation U which is controlled by a Boolean expression.

1. U is applied if and only if the Boolean expression is fulfilled.
2. U is first applied unconditionally. Then its inverse is applied if and only if the Boolean expression is not fulfilled.

In any case, an ODNF that is checked for is beneficial as its quantisation is straightforward: Each clause \mathcal{C} translates into a multi-controlled- U (resp. U^{-1}) where the control runs over all the qubits representing Boolean variables in \mathcal{C} . If the classical literal is positive, we control on whether the corresponding qubit is in the $|1\rangle$ state, otherwise whether it is in the $|0\rangle$ state. Because we assume an ODNF, we can ensure that U (resp. U^{-1}) is applied at most once when translating all the clauses into consecutive multi-controlled operations.

Gate count. For a given item cost z_m , we can now calculate the gate count for implementing the multi-controlled Hadamard gate $C_{\geq z_m}^B(H_b^{y_m})$. Following the first strategy of applying $H_b^{y_m}$ if and only if the remaining capacity covers z_m (that is if $x > z_m - 1$) and assuming

(i) as well as (iii), we obtain the count

$$\mathbf{G}_{\geq z_m}^{(1)} = \sum_{i=1}^{\lceil \log_2 z_m \rceil} (1 - (z_m - 1)_i) (2(\lceil \log_2 Z \rceil - i) + 1). \quad (34)$$

This implementation is favourable for costs z_m with comparatively many ones in the less significant bits of the binary representation of the number $z_m - 1$. Alternatively, following the second strategy, $H_b^{y_m}$ is first applied unconditionally (adding one to the gate count); then its inverse is applied if and only if the remaining capacity is strictly smaller than z_m . Again assuming (i) and (iii), this yields a total gate count of

$$\mathbf{G}_{\geq z_m}^{(2)} = 1 + \sum_{i=1}^{\lceil \log_2 z_m \rceil} (z_m)_i (2(\lceil \log_2 Z \rceil - i) + 1). \quad (35)$$

For the concrete circuit construction, we can then simply pick the implementation that requires fewer gates, i.e.,

$$\mathbf{G}_{\geq z_m} = \min \left(\mathbf{G}_{\geq z_m}^{(1)}, \mathbf{G}_{\geq z_m}^{(2)} \right). \quad (36)$$

The implementation of the reflection \mathcal{S}_0 is more straightforward: We simply have to check whether the profit register is in the state $|0\rangle^C$ and control the ancilla flip on the outcome. According to (i) and (iii), this yields a gate count of

$$\mathbf{G}_{=0} = 2\lceil \log_2 P \rceil - 1. \quad (37)$$

Lastly, the phase oracle is also realised as a single-qubit operation controlled on the truth value of a Boolean expression. The derivation of the gate count follows the same construction as for the multi-controlled Hadamard gate, with the only exception being that the phase oracle asks for a strict inequality “ $p > T$ ”. Hence we obtain

$$\mathbf{G}_{>T}^{(1)} = \sum_{i=1}^{\lceil \log_2 T \rceil} (1 - (T)_i) (2(\lceil \log_2 P \rceil - i) + 1), \quad (38)$$

$$\mathbf{G}_{>T}^{(2)} = 1 + \sum_{i=1}^{\lceil \log_2 T \rceil} (T + 1)_i (2(\lceil \log_2 P \rceil - i) + 1), \quad (39)$$

$$\mathbf{G}_{>T} = \min \left(\mathbf{G}_{>T}^{(1)}, \mathbf{G}_{>T}^{(2)} \right). \quad (40)$$

Cycle count. All the comparisons cannot be parallelised any further. Correspondingly, we have that

$$\mathbf{C}_{\geq z_m} = \mathbf{G}_{\geq z_m}, \quad (41)$$

$$\mathbf{C}_{=0} = \mathbf{G}_{=0}, \quad (42)$$

$$\mathbf{C}_{>T} = \mathbf{G}_{>T}. \quad (43)$$

6. QTG

After having detailed the resource estimations for all crucial subcircuits, we discuss now the overall gate and

cycle count for the entire QTG. We assume here the more resource-efficient version of the QTG that does not contain the last capacity update U_n^B .

Gate count. The total gate for QTG simply arises as the sum of the gates counts for the n controlled Hadamard gates U_m^A , the $n - 1$ capacity updates U_m^B , and the n profit updates U_m^C , i.e.,

$$\mathbf{G}_{\text{QTG}} = \sum_{m=1}^n \mathbf{G}_{\geq z_m} + \mathbf{G}_z + \mathbf{G}_p. \quad (44)$$

Cycle count. Up to this point, we have explored various methodologies to optimise the efficiency of gate and cycle counts for each component of the QTG. Now our focus shifts towards improving its overall cycle count. We take into account the following considerations:

- I. Parallelisation is not possible for the direct subtraction on the capacity register and the direct addition on the profit register, as they share the same control qubits.
- II. The addition operation on the profit register can be divided into two components, ADD_I and ADD_{II} , which can be executed simultaneously with the QFT_c and QFT_c^\dagger on the capacity register, respectively.
- III. The QFT_p on the profit register can be run in parallel with all the gates in the capacity register, as it does not involve any controlled operations.

Our first observation is, however, that the different layers $U_m = U_m^C U_m^B U_m^A$ have to be executed mutually disjointly as the subtraction in U_m^B and the addition in U_m^C are controlled by the qubits that the biased Hadamard gates in U_m^A act on. Therefore, no components commute across different layers, and we obtain

$$\mathbf{C}_{\text{QTG}} = \sum_{m=1}^n \mathbf{C}_m, \quad (45)$$

where \mathbf{C}_m denotes the cycle count per layer unitary U_m . Nevertheless, for a given item m we can apply additional parallelisation strategies within the layer U_m to reduce the total cycle count even further. The most complicated part is the first layer unitary U_1 , because it is the only one including QFTs on both the capacity and the cost register. [Figure 6](#) depicts all the different cases that can occur when trying to parallelise the subcircuits. In a nutshell, the number of cycles is determined by the length of the longest gate sequence – modulo the parallelisation assumptions/constraints I, II, and III – which can either be the circuit depth in the capacity or the profit register.

The other layer unitaries (except for the last one) are similarly constructed, but do not include any (inverse) QFT on the profit register. As the subcircuit U_m^A cannot be parallelised with the other components of U_m^B and U_m^C ,

we obtain – together with I and II – a cycle count of

$$\mathbf{C}_m = \mathbf{C}_{\geq z_m} + \mathbf{C}_{\text{DIRECT}_{z_m}} + \max(2\mathbf{C}_{\text{QFT-CAPACITY}}, \mathbf{C}_{\text{DIRECT}_{p_m}}). \quad (46)$$

The last layer unitary contains the inverse QFT for the profit register, but no cost subtraction in the capacity register. Therefore, we simply obtain

$$\mathbf{C}_n = \mathbf{C}_{\geq z_n} + \mathbf{C}_{\text{DIRECT}_{p_n}} + \mathbf{C}_{\text{QFT-PROFIT}}. \quad (47)$$

7. *QMaxSearch*

In contrast to the QTG whose gate and cycle count can be determined in advance the **QMaxSearch** routine has to be simulated to infer its total resource requirement. In order to derive a symbolic expression we assume that a run of **QMaxSearch** produces a sequence $(T_k)_{k=1}^R$ of intermediate thresholds with T_1 being the result of Integer Greedy. The search method is therefore not able to find a better total profit than T_R which might indicate that an optimal solution has been found. For each of these thresholds T_k , **QSearch** is executed, incorporating the comparison “ $P_y > T_k$ ” as phase oracle. Within a given instance of **QSearch** a sequence $(j_\ell^{(k)})_{\ell=1}^{S(k)}$ of powers is constructed such that the termination condition

$$\sum_{\ell=1}^{S(R)-1} 2j_\ell^{(R)} + 1 < M, \quad \sum_{\ell=1}^{S(R)} 2j_\ell^{(R)} + 1 \geq M \quad (48)$$

holds in the last application of **QSearch**. For all prior iterations the termination condition is never triggered, because an improved threshold is found, respectively.

Gate count. From the knowledge about the threshold T_k and the corresponding power sequence we can now determine the gate count of the k -th iteration of **QSearch**: Before applying \mathcal{Q} with a given power j the QTG is applied once to create the initial superposition of feasible states. The definition (10) of the Amplitude Amplification operator immediately gives rise to its gate count

$$\mathbf{G}_{\mathcal{Q}_k} = 2\mathbf{G}_{\text{QTG}} + \mathbf{G}_{=0} + \mathbf{G}_{>T_k}. \quad (49)$$

Multiplying the latter with the respective power and summing over all powers we obtain for the k -th iteration of **QSearch** a gate count of

$$\mathbf{G}_{\text{QSearch}_k} = \sum_{\ell=1}^{S(k)} (2j_\ell^{(k)} + 1)\mathbf{G}_{\text{QTG}} + j_\ell^{(k)}(\mathbf{G}_{=0} + \mathbf{G}_{>T_k}). \quad (50)$$

The total gate count of **QMaxSearch** is then given by

$$\mathbf{G}_{\text{QMaxSearch}} = \sum_{k=1}^R \mathbf{G}_{\text{QSearch}_k}. \quad (51)$$

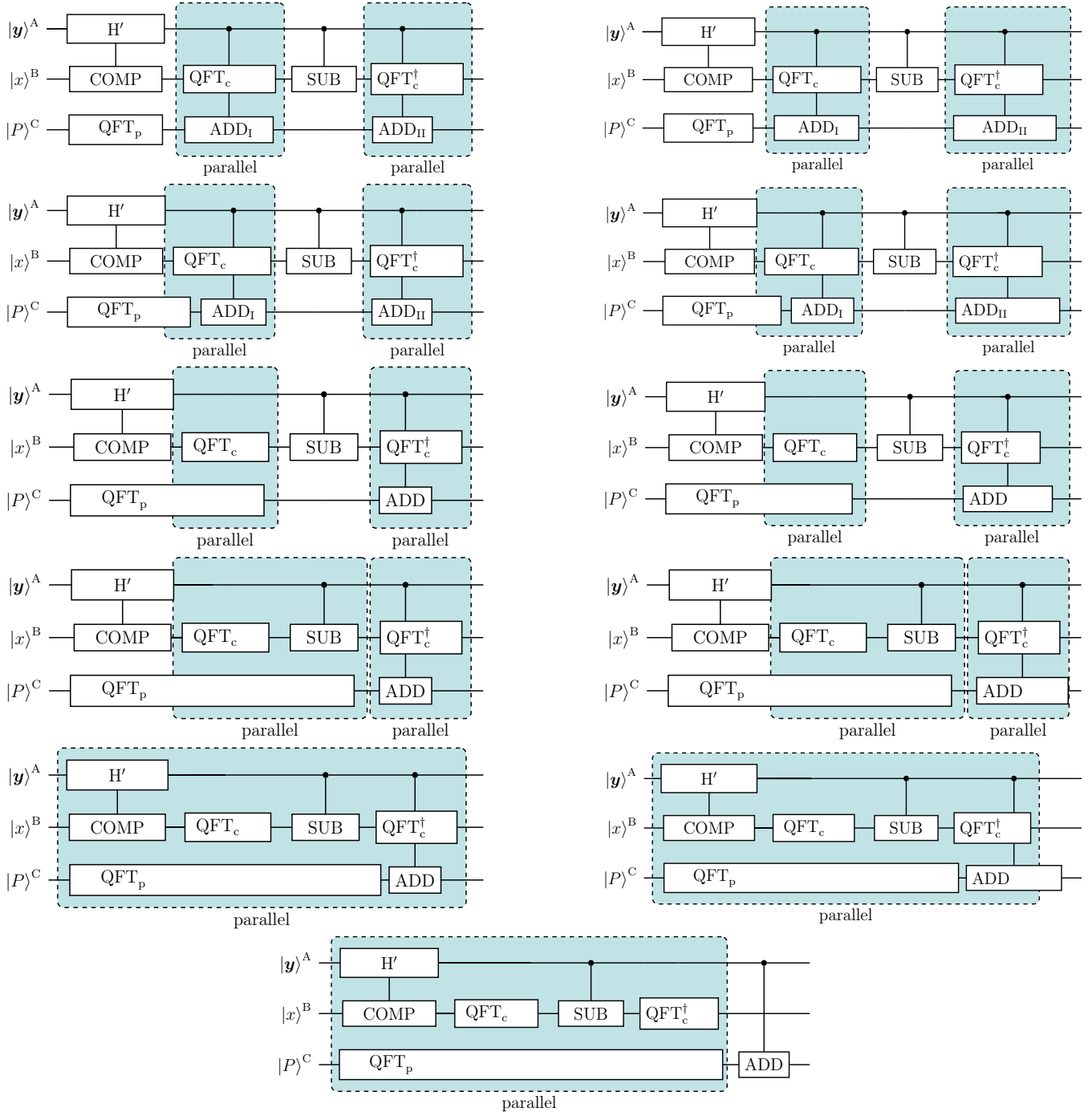


FIG. 6. All possible parallelisation outcomes for the first layer unitary U_1 within the QTG.

Cycle count. Because the operators \mathcal{S}_0 and $\mathcal{S}_{P_y > T_k}$ are controlled on the profit register's qubits no further parallelisation within Q is possible. Therefore, we obtain for the **QSearch** cycle count

$$\mathbf{C}_{\text{QSearch}_k} = \sum_{\ell=1}^{S(k)} (2j_\ell^{(k)} + 1) \mathbf{C}_{\text{QTG}} + j_\ell^{(k)} (\mathbf{C}_{=0} + \mathbf{C}_{>T_k}) \quad (52)$$

and, analogously, for the final cycle count of the entire **QMaxSearch** routine

$$\mathbf{C}_{\text{QMaxSearch}} = \sum_{k=1}^R \mathbf{C}_{\text{QSearch}_k}. \quad (53)$$

The formula (53) is precisely what is being used for calculating the elapsed quantum cycles in [Figure 2 a](#)).